






Generation of metastable krypton using a 124-nm laserX.-Z. Dong , F. Ritterbusch,^{*} D.-F. Yuan , J.-W. Yan, W.-T. Chen, W. Jiang,
Z.-T. Lu ,[†] J. S. Wang , X.-A. Wang,[‡] and G.-M. Yang *University of Science and Technology of China, 96 Jinzhai Road, Hefei 230026, China*

(Received 15 June 2021; accepted 18 February 2022; published 9 March 2022)

We have realized the optical excitation of krypton to a metastable level with an efficiency as high as 23 % using near-resonant 124-nm light produced by four-wave mixing in mercury vapor. Self-absorption in mercury is circumvented by adjusting the detuning and phase matching according to experimental and theoretical characterizations. Density-matrix calculations of the metastable krypton generation agree with the measured dependencies of the excitation efficiency, indicating pathways towards a further improvement. The obtained excitation efficiency, being one order of magnitude higher than that of previously demonstrated techniques, enables an extension of the metastable density regime for atomic physics applications, including magnetometry, atom lithography, and radioisotope dating.

DOI: [10.1103/PhysRevA.105.L031101](https://doi.org/10.1103/PhysRevA.105.L031101)

Introduction. Noble-gas atoms have found a wide range of applications in atomic physics such as lithography [1,2], Bose-Einstein condensation [3,4], cold collision studies [5,6], and other fundamental physics experiments [7–9]. The long-lived radioisotopes of krypton and argon are particularly useful tracers in the earth sciences, and are detected with the atom trap trace analysis (ATTA) method [10,11]. All of these applications employ noble-gas atoms in a metastable level due to a large internal energy or due to the lack of suitable lasers at the required vacuum ultraviolet (VUV) wavelength (100–200 nm) for ground-level transitions. At present, the generation of metastable noble-gas atoms is commonly achieved by electron-impact excitation in a gas discharge [12,13]. Unfortunately, electron-atom collisions in the discharge simultaneously destroy metastable atoms via deexcitation and ionization [14–16], leading to a metastable population fraction at an equilibrium of only 10^{-4} – 10^{-3} . Moreover, implantation into and sputtering of the surfaces surrounding the discharge can cause detrimental effects.

These limitations of the discharge excitation can be overcome by optically transferring the atoms from the ground to the metastable level. For krypton, one such path is via two-photon excitation from the ground state to the excited $2p_6$ using 215 nm + 215 nm, followed by a spontaneous decay to the metastable $1s_5$. This mechanism has recently been demonstrated in a spectroscopy cell using a pulsed optical parametric oscillator laser [17]. Metastable-generation efficiencies up to 2% per pulse (pulse energy 2 mJ, pulse length 5 ns) were achieved in a focal region of 0.1 mm diameter and 1 mm length. The efficiencies were observed to be saturating due to the ionization loss induced by the high laser intensity, which is necessary for this scheme because the intermediate state for the two-photon transition is far from resonance. The

power requirement can be significantly lowered by using two-photon excitation with a near-resonant intermediate state via the 124- and 819-nm transition [Fig. 1(c)]. So far, the generation of bright and resonant 124-nm light has posed a major difficulty for employing this scheme. Metastable generation with an efficiency comparable to that of discharge excitation was demonstrated using 124-nm light generated by a krypton discharge lamp [18–22]. However, this approach has so far not overcome the limited excitation efficiency and suffers from decreasing transmission of the output MgF_2 window due to sputtering processes in the discharge lamp. An alternative source of the 124-nm light is a free-electron laser [23], which may become a viable option once facilities with high power and high repetition rates are realized.

A table-top approach to produce coherent VUV light is via four-wave mixing (FWM) in a dispersive medium, typically a metal vapor or noble gas [24–29]. Mercury is a convenient medium due to its high vapor pressure at moderate temperatures. It is especially suitable for producing tunable light around 120 nm because the high-lying n^1P levels with $n > 8$ contribute to a near-resonant three-photon process [26–30]. In this Letter, we have optically excited krypton with 124-nm light produced by four-wave mixing in a mercury vapor using pulsed dye lasers. The resulting 124-nm light with a pulse energy of $\sim 2 \mu\text{J}$ is combined with pulsed 819-nm light in a cell for the generation of metastable krypton. The theoretical calculations for the FWM process as well as the metastable krypton generation are in good agreement with the measurements, indicating ways to further increase the excitation efficiency.

Experimental setup. A schematic of the experimental setup and the relevant transitions in mercury and krypton are shown in Fig. 1. The setup consists of two main parts: a mercury cell for the production of 124-nm light by FWM and a krypton cell for the generation of metastable krypton. The three fundamental beams for FWM are supplied by dye lasers that are pumped by a Nd:YAG laser at a repetition rate of 20 Hz. The 253-nm UV light is produced by frequency dou-

^{*}florian@ustc.edu.cn[†]ztlu@ustc.edu.cn[‡]xawang@ustc.edu.cn

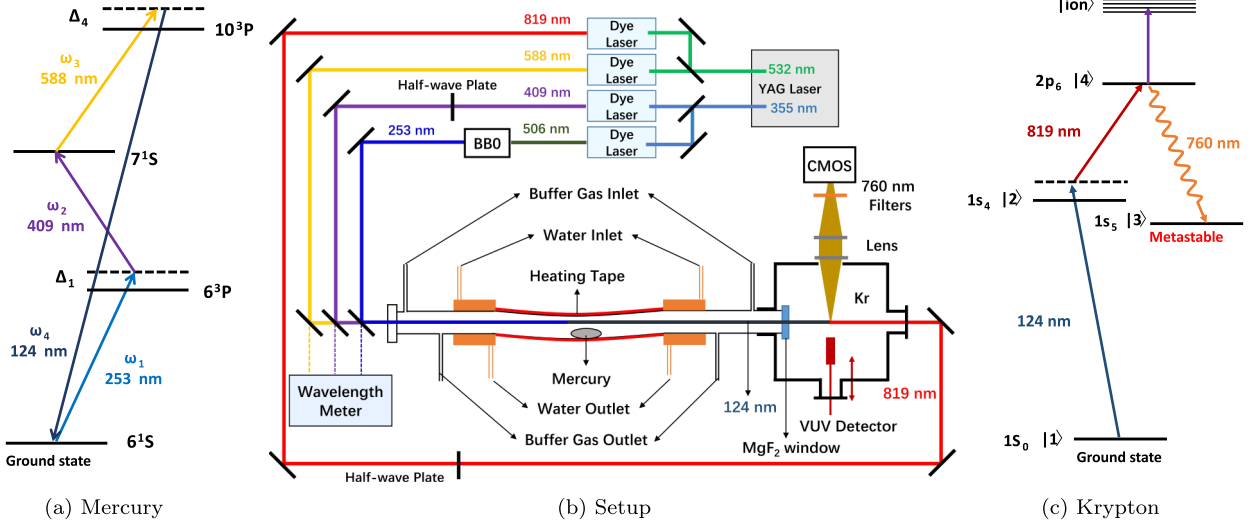


FIG. 1. (a) Energy-level scheme for the production of 124-nm light by FWM in mercury. (b) Setup for FWM and metastable krypton generation. (c) Schematic of the relevant multilevel system in krypton.

bling in a beta barium borate (BBO) crystal. Typical pulse energies of the 253-, 409-, and 588-nm fundamental beams are 2, 5, and 15 mJ, respectively. The beams have a diameter of 2-3 mm. The pulse length is ~ 10 ns and the bandwidth is ~ 4 GHz. The mercury cell is similar to that described in Ref. [28].

The krypton cell is filled with 2×10^{-4} mbar krypton gas. The produced 124-nm beam as well as the fundamental beams enter the krypton cell through a MgF_2 window. The 124-nm pulse energy is measured via the photoelectric emission from a biased platinum plate [28,31], which can be moved in and out of the VUV beam. The 819-nm beam is overlapped with the 124-nm beam in the krypton cell. The 760-nm photons emitted upon the decay of a krypton atom to the $1s_5$, are imaged onto a complementary metal-oxide semiconductor (CMOS) camera as a signal for metastable generation. The stray light from the fundamental beams is suppressed by three successive 760-nm bandpass filters. From the camera signal the number of metastable atoms can be calculated via the known quantum efficiency of the camera and the solid angle of the imaging optics.

Production of 124-nm light by FWM. The relevant energy levels of mercury are shown in Fig. 1(a). The VUV power P_4 produced by FWM using three unfocused fundamental beams is given by [26]

$$P_4 \propto P_1 P_2 P_3 \left| \frac{\chi^{(3)} \omega_4 N L \sin(NL\Delta k/2)}{A(NL\Delta k/2)} \right|^2, \quad (1)$$

where $P_{1,2,3}$ are the powers of the three incident fundamental beams, ω_4 is the angular frequency of the produced VUV light, L and A are the interaction length and area, N is the atomic number density of mercury, and $\chi^{(3)}$ is the third-order nonlinear susceptibility. Δk is the phase mismatch defined as $\Delta k = [k(\omega_4) - k(\omega_3) - k(\omega_2) - k(\omega_1)]/N$, where $k(\omega_i) = \omega_i/c \text{Re}\sqrt{1 + \chi^{(1)}(\omega_i)}$ denotes the wave vector of the corresponding light with angular frequency ω_i and $\chi^{(1)}$ is the first-order susceptibility. P_4 is maximum for $\Delta k = 0$, i.e., for

perfect phase matching. The phase mismatch can be minimized by tuning Δ_4 and Δ_1 (see Supplemental Material [32]), i.e., the detunings of the laser light with respect to the 10^3P and 6^3P transitions, respectively (see Fig. 1). As evident from Eq. (1), another important factor that determines the output power is the third-order nonlinear susceptibility $\chi^{(3)}$. It is maximum if $\omega_1 + \omega_2$ is resonant with the 6^1S - 7^1P transition, a resonance condition maintained throughout this work. Moreover, $\chi^{(3)}$ increases if the detunings Δ_4 and Δ_1 decrease (see Supplemental Material [32]).

Metastable krypton generation. The multilevel system relevant for the dynamic evolution of the metastable krypton generation is depicted in Fig. 1(c). Besides the bound levels, an ionization continuum is also included. The krypton atoms are driven by 124- and 819-nm light pulses. The time evolution of the density-matrix elements ρ_{jl} is governed by the Lindblad master equation [33]

$$\dot{\rho}_{jl} = -\frac{i}{\hbar} [\hat{H}(t), \rho_{jl}(t)] + \hat{\mathcal{L}}(\gamma_{jl}, \rho_{jl}(t)), \quad (2)$$

where $\hat{H}(t)$ is the Hamilton operator for the coherent atom-light interaction, and $\hat{\mathcal{L}}$ is the Lindblad operator, which accounts for the incoherent processes. γ_{jl} represents the damping rates of the coherences caused by spontaneous decay, phase fluctuations of the laser light, and photoionization. The phase fluctuation of the laser light can be described by the phase diffusion model [34,35] and leads to the effective damping rates

$$\Gamma_L = \sigma_L \frac{(b\sigma_L)^2}{\Delta_L^2 + (b\sigma_L)^2}, \quad (3)$$

where σ_L is the full width at half maximum (FWHM) linewidth of the laser, b is the line-shape parameter, and Δ_L is the detuning of the laser. Photoionization from $1s_4$ and $1s_5$ can be neglected, as the cross sections are two orders of magnitude lower than that from $2p_6$ [36,37]. The photoionization cross section from $2p_6$ is the highest around 480 nm and decreases

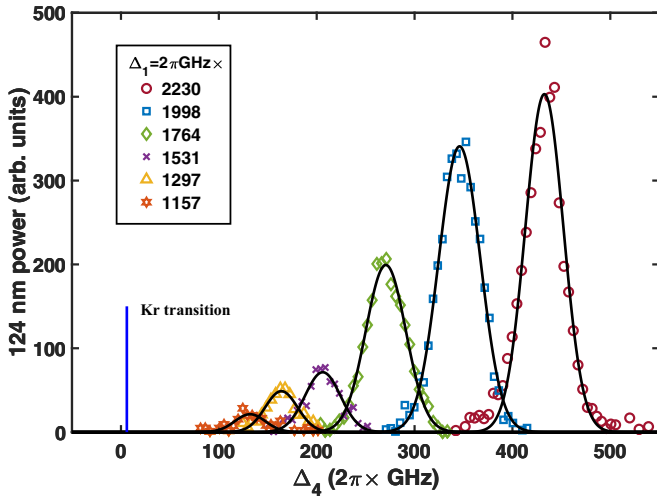


FIG. 2. 124-nm power as a function of the VUV detuning Δ_4 for different UV detunings Δ_1 . The black lines serve as a guide to the eye.

for shorter wavelength [36,37]. Moreover, in this work the intensity of the 409-nm light in the interaction region is much higher than that of the 124- and 253-nm light. As a result, photoionization can be assumed to occur only from $2p_6$ and induced only by the 409-nm light. Taking into account all the damping rates, the differential equations (2) are solved numerically with the initial condition of krypton atoms in the ground state (see the Supplemental Material [32] for more details).

Results and discussion. The resonance of the 124-nm transition in krypton is only 7 GHz away from that of the 124-nm transition in mercury (Fig. 2), which poses a challenge due to self-absorption. We measure the output power as a function of VUV detuning Δ_4 for different UV detunings Δ_1 (Fig. 2). $\omega_1 + \omega_2$ is always kept on resonance with the 6^1S-7^1P transition and Δ_4 is scanned by adjusting ω_3 . For each Δ_1 there is an optimum Δ_4 for which the VUV power is the highest, as expected from the theory (see Supplemental Material [32]).

As the VUV detuning Δ_4 decreases, the VUV output power should increase but actually decreases due to the strong absorption of the VUV light in the mercury cell. It is apparent that the frequency needed for the resonant excitation of krypton, being only 7 GHz away from the mercury transition 10^1P , cannot be reached. We choose a blue detuning of +430 GHz to the $1s_4$ level of krypton (i.e., blue detuning of $\Delta_4 = +437$ GHz to the mercury transition) as the best compromise between high VUV power and small detuning. At this detuning, we obtain a 124-nm pulse energy of $2 \mu\text{J}$.

For the generation of metastable krypton in the cell, the VUV detector is retracted such that the 819-nm beam overlaps with the 124-nm beam in the center of the cell (Fig. 1). On the camera we observe the spatially resolved 760-nm fluorescence from the generation of metastable krypton (Fig. 3). From the signal we deduce the number of emitted photons and thus the number of produced metastable krypton atoms (see Supplemental Material [32]). By comparing with the total number of krypton atoms in the cell derived from the gas pressure, we obtain the metastable excitation efficiency. The theoretic

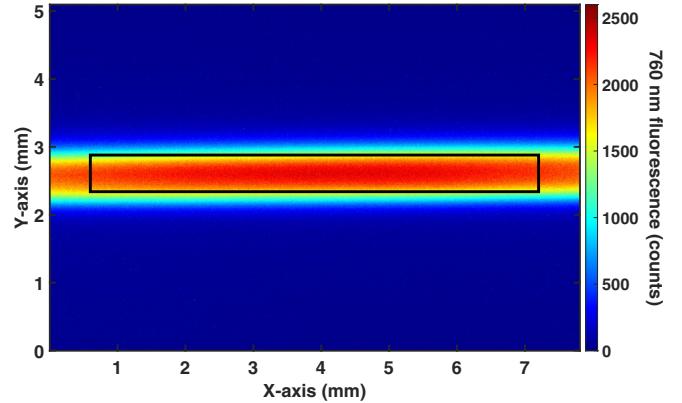


FIG. 3. Camera image of the 760-nm fluorescence emitted upon the generation of metastable krypton. The signal is averaged over 40 pulses in an integration time of 2 s. The black box indicates the analysis region of 0.6 mm diameter and 6.6 mm length.

cal excitation efficiency is obtained from the density-matrix calculations according to Eq. (2). The metastable excitation efficiencies as a function of two-photon detuning (representing the energy difference between the $1S_0-2p_6$ transition and the sum of the two photons, one at 124 nm and the other at 819 nm), from both the measurement and the density-matrix calculation, are shown in Fig. 4(a) for different 819-nm pulse energies. The measured line shape is asymmetric around the resonance with the asymmetry becoming more prominent as the 819-nm pulse energy increases. This trend is reproduced by the line shapes calculated based on Eq. (2). As we can identify via density-matrix calculations, the asymmetry is caused by photoionization (due to the 409-nm beam) in combination with power broadening and the ac Stark shift induced by the 819-nm beam.

The measured metastable generation efficiencies as a function of 819- and 124-nm pulse energies are shown in Figs. 4(b) and 4(c). The excitation efficiency saturates at the available 819-nm pulse energy of 10 mJ. However, it keeps increasing with the 124-nm pulse energy up to 23%, the maximum excitation efficiency achieved in this work, indicating the potential to obtain even higher metastable excitation efficiencies at higher VUV power. The measurements are in good agreement with the density-matrix calculations using a 12-GHz linewidth for the produced 124-nm light and a line-shape factor $b = 3$. We observe photoionization only from the 409-nm beam, in agreement with the considerations given above. Here, the 409-nm power has been tuned to the best compromise between reducing photoionization loss and increasing the 124-nm output. In future experiments the photoionization can be suppressed by spatially separating the 124-nm beam from the fundamental beams, which would increase the excitation efficiency from 23% to $\sim 30\%$. We do not observe a significant decrease of the MgF_2 window transmission over the course of the measurements (several weeks) presented here. This is a considerable advantage over the discharge lamp approach, where the transmission decreases substantially over a short time (several days) due to sputtering processes in the discharge lamp [18–22].

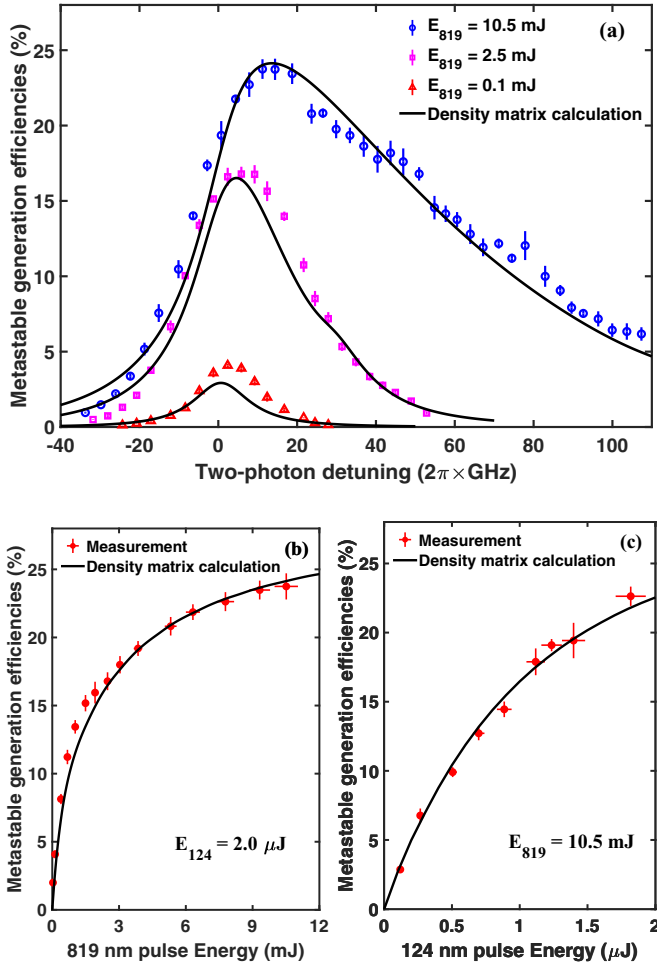


FIG. 4. Metastable generation efficiency vs (a) two-photon detuning, (b) 819-nm pulse energy, and (c) 124-nm pulse energy. The two-photon detuning is scanned by changing the detuning of the 819-nm light.

Conclusion and outlook. We have realized the laser-based optical generation of metastable krypton with excitation efficiencies as high as 23%. This is two orders of magnitude higher than that reached by the commonly used discharge techniques. Compared to the previous demonstration of metastable krypton generation via two-photon excitation (215 nm + 215 nm) [17], this work improved the efficiency by one order of magnitude and expanded the excitation volume by at least two orders of magnitude. As Fig. 4 indicates, the excitation efficiency can be further enhanced by increasing the 124-nm power, e.g., by adding a second pump laser or by redesigning the mercury cell to reduce the 124-nm self-absorption. The latter would also allow the 124-nm light to be tuned closer to the krypton resonance, which would drastically reduce the 124-nm power required for the two-photon excitation.

The excitation method demonstrated here is optical, so it avoids the limitations associated with ionization, which inevitably occurs in the discharge excitation. This is a substan-

tial improvement for applications such as radiokrypton dating of small polar ice core samples in the context of reconstructing climate history [38–40], as it alleviates the cross-sample contamination due to sputtering processes in the ATTA discharge source.

The method demonstrated here for krypton can also be used for the generation of metastable argon [41]. This is of particular interest for radioargon dating of environmental water and ice samples using ATTA [42–46], where precision, sample size, and sample throughput are currently limited by cross-sample contamination as well as the low ^{39}Ar count rate [47]. For the production of metastable xenon [48], magnesium is preferred over mercury as the FWM medium. In particular for ^{129}Xe , an important isotope for magnetic resonance imaging (MRI) and comagnetometry in fundamental physics experiments [49,50], the metastable generation method presented here has the potential to realize hyperpolarization via metastable exchange optical pumping [51–53]. In the same way ^{83}Kr , a promising surface-sensitive magnetic resonance imaging (MRI) contrast agent for the diagnosis of pulmonary diseases, may be hyperpolarized as well [54,55].

The 124-nm light produced in this experiment is pulsed, so for metastable krypton beam experiments the downstream application needs to be adapted, as realized in previous pulsed metastable beam experiments [5,56]. At a repetition rate of 20 Hz and a travel time of $\sim 30 \mu\text{s}$ for the atoms to refill a 6.6-mm-long excitation region, the excitation efficiency reached here in the cell during the duty cycle translates to a time-averaged excitation efficiency of $\sim 1.4 \times 10^{-4}$ for a metastable krypton beam. This is comparable to the efficiency reached with the commonly used discharge excitation. The overall excitation efficiency can be substantially increased by pulsing the atomic beam synchronously with the light [6,57]. As the excitation method presented in this work is laser based, it allows for spatial and temporal control of the metastable production. This is instrumental for pulsed nozzle beam sources, which are particularly suited to experiments where a narrow atomic velocity distribution is desired such as in atom lithography [58–60]. Another way to increase the overall excitation efficiency is by switching to a laser system with a higher repetition rate. Recent developments in laser technology feature repetition rates in the kHz range at sufficient pulse energies [61,62], allowing a two orders of magnitude higher overall metastable generation efficiency. Hence, by employing existing vacuum and laser technology it is feasible to reach an overall excitation efficiency for a krypton beam comparable to the excitation efficiency obtained in this work in a cell. This represents a major advance for applications that require a high metastable beam flux, such as atom lithography, cold collision studies, or noble-gas radioisotope dating using the atom trap trace analysis method.

Acknowledgments. This work is funded by the National Key Research and Development Program of China (2016YFA0302200), National Natural Science Foundation of China (41727901, 41961144027, 41861224007), Anhui Initiative in Quantum Information Technologies (AHY110000), and Chinese Academy of Sciences (Grant No. XDB 17010000).

- [1] K. K. Berggren, A. Bard, J. L. Wilbur, J. D. Gillaspay, A. G. Helg, J. J. McClelland, S. L. Rolston, W. D. Phillips, M. Prentiss, and G. M. Whitesides, *Science* **269**, 1255 (1995).
- [2] T. Nesse, I. Simonsen, and B. Holst, *Phys. Rev. Appl.* **11**, 024009 (2019).
- [3] A. Robert, O. Sirjean, A. Browaeys, J. Poupard, S. Nowak, D. Boiron, C. I. Westbrook, and A. Aspect, *Science* **292**, 461 (2001).
- [4] R. I. Khakimov, B. M. Henson, D. K. Shin, S. S. Hodgman, R. G. Dall, K. G. H. Baldwin, and A. G. Truscott, *Nature (London)* **540**, 100 (2016).
- [5] A. B. Henson, S. Gersten, Y. Shagam, J. Narevicius, and E. Narevicius, *Science* **338**, 234 (2012).
- [6] S. D. S. Gordon, J. J. Omiste, J. Zou, S. Tanteri, P. Brumer, and A. Osterwalder, *Nat. Chem.* **10**, 1190 (2018).
- [7] W. Vassen, C. Cohen-Tannoudji, M. Leduc, D. Boiron, C. I. Westbrook, A. Truscott, K. Baldwin, G. Birkl, P. Cancio, and M. Trippenbach, *Rev. Mod. Phys.* **84**, 175 (2012).
- [8] Y. Huisman, A. Rouze, A. Gijsbertsen, J. H. Jungmann, A. S. Smolkowska, P. S. W. M. Logman, F. Lpine, C. Cauchy, S. Zamith, T. Marchenko, J. M. Bakker, G. Berden, B. Redlich, A. F. G. van der Meer, H. G. Muller, W. Vermin, K. J. Schafer, M. Spanner, M. Y. Ivanov, O. Smirnova *et al.*, *Science* **331**, 61 (2011).
- [9] J. Tomkovi, M. Schreiber, J. Welte, M. Kiffner, J. Schmiedmayer, and M. K. Oberthaler, *Nat. Phys.* **7**, 379 (2011).
- [10] C. Y. Chen, Y. M. Li, K. Bailey, T. P. Connor, L. Young, and Z. T. Lu, *Science* **286**, 1139 (1999).
- [11] Z. T. Lu, P. Schlosser, W. M. Smethie, N. C. Sturchio, T. P. Fischer, B. M. Kennedy, R. Purtschert, J. P. Severinghaus, D. K. Solomon, T. Tanhua, and R. Yokochi, *Earth-Sci. Rev.* **138**, 196 (2014).
- [12] J. Kawanaka, M. Hagiuda, K. Shimizu, F. Shimizu, and H. Takuma, *Appl. Phys. B* **56**, 21 (1993).
- [13] C. Y. Chen, K. Bailey, Y. M. Li, T. P. O'Connor, Z. T. Lu, X. Du, L. Young, and G. Winkler, *Rev. Sci. Instrum.* **72**, 271 (2001).
- [14] H. A. Hyman, *Phys. Rev. A* **18**, 441 (1978).
- [15] H. A. Hyman, *Phys. Rev. A* **20**, 855 (1979).
- [16] A. A. Mityureva and V. V. Smirnov, *Opt. Spectrosc.* **128**, 443 (2020).
- [17] M. A. Dakka, G. Tsiminis, R. D. Glover, C. Perrella, J. Moffatt, N. A. Spooner, R. T. Sang, P. S. Light, and A. N. Luiten, *Phys. Rev. Lett.* **121**, 093201 (2018).
- [18] L. Young, D. Yang, and R. W. Dunford, *J. Phys. B: At., Mol. Opt. Phys.* **35**, 2985 (2002).
- [19] Y. Ding, S. M. Hu, K. Bailey, A. M. Davis, R. W. Dunford, Z. T. Lu, T. P. O'Connor, and L. Young, *Rev. Sci. Instrum.* **78**, 023103 (2007).
- [20] H. Daerr, M. Kohler, P. Sahling, S. Tippenhauer, A. Arabi-Hashemi, C. Becker, K. Sengstock, and M. B. Kalinowski, *Rev. Sci. Instrum.* **82**, 073106 (2011).
- [21] M. Kohler, H. Daerr, P. Sahling, C. Sieveke, N. Jerschabek, M. B. Kalinowski, C. Becker, and K. Sengstock, *Europhys. Lett.* **108**, 13001 (2014).
- [22] J. S. Wang, F. Ritterbusch, X. Z. Dong, C. Gao, H. Li, W. Jiang, S. Y. Liu, Z. T. Lu, W. H. Wang, G. M. Yang, Y. S. Zhang, and Z. Y. Zhang, *Phys. Rev. Lett.* **127**, 023201 (2021).
- [23] Y. Chang, Y. Yu, H. Wang, X. Hu, Q. Li, J. Yang, S. Su, Z. He, Z. Chen, L. Che, X. Wang, W. Zhang, G. Wu, D. Xie, M. N. R. Ashfold, K. Yuan, and X. Yang, *Nat. Commun.* **10**, 1250 (2019).
- [24] S. E. Harris and R. B. Miles, *Appl. Phys. Lett.* **19**, 385 (1971).
- [25] R. Hilbig and R. Wallenstein, *IEEE J. Quantum Electron.* **17**, 1566 (1981).
- [26] A. V. Smith and W. J. Alford, *J. Opt. Soc. Am. B* **4**, 1765 (1987).
- [27] D. R. Albert, D. L. Proctor, and H. F. Davis, *Rev. Sci. Instrum.* **84**, 063104 (2013).
- [28] J. Wang, F. Liu, Y. Mo, Z. Wang, S. Zhang, and X. Zhang, *Rev. Sci. Instrum.* **88**, 114102 (2017).
- [29] D. Kolbe, M. Scheid, and J. Walz, *Phys. Rev. Lett.* **109**, 063901 (2012).
- [30] A. V. Smith and W. J. Alford, *Phys. Rev. A* **33**, 3172 (1986).
- [31] W. C. Walker, N. Wainfan, and G. L. Weissler, *J. Appl. Phys.* **26**, 1366 (1955).
- [32] See Supplemental Material at <http://link.aps.org/supplemental/10.1103/PhysRevA.105.L031101> for more details on the density-matrix calculation of the metastable krypton generation,
- [33] G. Lindblad, *Commun. Math. Phys.* **48**, 119 (1976).
- [34] A. T. Georges and P. Lambropoulos, *Phys. Rev. A* **18**, 587 (1978).
- [35] P. Zoller and P. Lambropoulos, *J. Phys. B: At., Mol. Opt. Phys.* **12**, L547 (1979).
- [36] H. A. Hyman, *Appl. Phys. Lett.* **31**, 14 (1977).
- [37] C. Duzy and H. A. Hyman, *Phys. Rev. A* **22**, 1878 (1980).
- [38] J. Severinghaus, E. W. Wolff, and E. J. Brook, *EOS, Trans. Am. Geophys. Union* **91**, 357 (2010).
- [39] J. M. Schaefer, R. C. Finkel, G. Balco, R. B. Alley, M. W. Caffee, J. P. Briner, N. E. Young, A. J. Gow, and R. Schwartz, *Nature (London)* **540**, 252 (2016).
- [40] L. G. Thompson, T. Yao, M. E. Davis, K. A. Henderson, E. Mosley-Thompson, P.-N. Lin, J. Beer, H.-A. Synal, J. Cole-Dai, and J. F. Bolzan, *Science* **276**, 1821 (1997).
- [41] C. H. Kwon, H. L. Kim, and M. S. Kim, *Rev. Sci. Instrum.* **74**, 2939 (2003).
- [42] W. Jiang, W. Williams, K. Bailey, A. M. Davis, S. M. Hu, Z. T. Lu, T. P. O'Connor, R. Purtschert, N. C. Sturchio, Y. R. Sun, and P. Mueller, *Phys. Rev. Lett.* **106**, 103001 (2011).
- [43] F. Ritterbusch, S. Ebser, J. Welte, T. Reichel, A. Kersting, R. Purtschert, W. Aeschbach-Hertig, and M. K. Oberthaler, *Geophys. Res. Lett.* **41**, 6758 (2014).
- [44] S. Ebser, A. Kersting, T. Stven, Z. Feng, L. Ringena, M. Schmidt, T. Tanhua, W. Aeschbach, and M. K. Oberthaler, *Nat. Commun.* **9**, 5046 (2018).
- [45] Z. Feng, P. Bohleber, S. Ebser, L. Ringena, M. Schmidt, A. Kersting, P. Hopkins, H. Hoffmann, A. Fischer, W. Aeschbach, and M. K. Oberthaler, *Proc. Natl. Acad. Sci. USA* **116**, 8781 (2019).
- [46] M. Holzer, T. DeVries, and W. Smethie, Jr., *Geophys. Res. Lett.* **46**, 7491 (2019).
- [47] A. L. Tong, J.-Q. Gu, G.-M. Yang, S.-M. Hu, W. Jiang, Z.-T. Lu, and F. Ritterbusch, *Rev. Sci. Instrum.* **92**, 063204 (2021).
- [48] S. C. Wallace and G. Zdasiuk, *Appl. Phys. Lett.* **28**, 449 (1976).
- [49] A. S. Khan, R. L. Harvey, J. R. Birchall, R. K. Irwin, P. Nikolaou, G. Schrank, K. Emami, A. Dummer, M. J. Barlow, B. M. Goodson, and E. Y. Chekmenev, *Angew. Chem., Int. Ed.* **60**, 22126 (2021).
- [50] N. Sachdeva, I. Fan, E. Babcock, M. Burghoff, T. E. Chupp, S. Degenkolb, P. Fierlinger, S. Haude, E. Kraegeloh, W. Kilian,

- S. Knappe-Grüneberg, F. Kuchler, T. Liu, M. Marino, J. Meinel, K. Rolfs, Z. Salhi, A. Schnabel, J. T. Singh, S. Stuibler *et al.*, *Phys. Rev. Lett.* **123**, 143003 (2019).
- [51] T. Xia, S. W. Morgan, Y. Y. Jau, and W. Happer, *Phys. Rev. A* **81**, 033419 (2010).
- [52] T. Chupp and S. Swanson, Medical imaging with laser-polarized noble gases, in *Advances in Atomic, Molecular, and Optical Physics*, edited by B. Bederson and H. Walther (Academic, New York, 2001), Vol. 45, pp. 41–98.
- [53] T. R. Gentile, P. J. Nacher, B. Saam, and T. G. Walker, *Rev. Mod. Phys.* **89**, 045004 (2017).
- [54] G. E. Pavlovskaya, Z. I. Cleveland, K. F. Stupic, R. J. Basaraba, and T. Meersmann, *Proc. Natl. Acad. Sci. USA* **102**, 18275 (2005).
- [55] N. J. Rogers, F. Hill-Casey, K. F. Stupic, J. S. Six, C. Lesbats, S. P. Rigby, J. Fraissard, G. E. Pavlovskaya, and T. Meersmann, *Proc. Natl. Acad. Sci. USA* **113**, 3164 (2016).
- [56] W. Jiang, K. Bailey, Z. T. Lu, P. Mueller, T. P. OConnor, C. F. Cheng, S. M. Hu, R. Purtschert, N. C. Sturchio, Y. R. Sun, W. D. Williams, and G. M. Yang, *Geochim. Cosmochim. Acta* **91**, 1 (2012).
- [57] U. Even, *EPJ Tech. Instrum.* **2**, 17 (2015).
- [58] D. Meschede and H. Metcalf, *J. Phys. D* **36**, R17 (2003).
- [59] C. S. Allred, J. Reeves, C. Corder, and H. Metcalf, *J. Appl. Phys.* **107**, 033116 (2010).
- [60] S. D. Eder, T. Reisinger, M. M. Greve, G. Bracco, and B. Holst, *New J. Phys.* **14**, 073014 (2012).
- [61] Z.-W. Fan, J.-S. Qiu, Z.-J. Kang, Y.-Z. Chen, W.-Q. Ge, and X.-X. Tang, *Light: Sci. Appl.* **6**, e17004 (2017).
- [62] L. Liu, N. Li, Y. Liu, C. Wang, W. Wang, and H. Huang, *Opt. Express* **29**, 22008 (2021).